Article

De-hydrogenation/Rehydrogenation Properties and Reaction Mechanism of $A_mZn(NH_2)_n$-$2n$LiH Systems (A = Li, K, Na, and Rb)

Hujun Cao [1,2], Claudio Pistidda [1,*], Theresia M. M. Richter [3], Giovanni Capurso [1], Chiara Milanese [4], Jo-Chi Tseng [5], Yuanyuan Shang [1], Rainer Niewa [3], Ping Chen [2], Thomas Klassen [1] and Martin Dornheim [1,*]

1 Institute of Hydrogen Technology, Materials Technology, Helmholtz-Zentrum Hereon GmbH, Max-Planck-Straße 1, 21502 Geesthacht, Germany; caohujun@dicp.ac.cn (H.C.); giovanni.capurso@hereon.de (G.C.); yuanyuan.shang@hereon.de (Y.S.); thomas.klassen@hereon.de (T.K.)
2 Dalian National Laboratory for Clean Energy Dalian Institute of Chemical Physics, Chinese Academy of Sciences, Dalian 116023, China; pchen@dicp.ac.cn
3 Institute of Inorganic Chemistry, University Stuttgart, Pfaffenwaldring 55, 70569 Stuttgart, Germany; richter.theresia@yahoo.de (T.M.M.R.); rainer.niewa@iac.uni-stuttgart.de (R.N.)
4 Pavia H2 Lab, C.S.G.I. & Department of Chemistry, Physical Chemistry Section, University of Pavia, Viale Taramelli 16, I-27100 Pavia, Italy; chiara.milanese@unipv.it
5 Deutsches Elektronen-Synchrotron (DESY), Notkestraße 85, 22607 Hamburg, Germany; jochi@mpi-muelheim.mpg.de
* Correspondence: claudio.pistidda@hereon.de (C.P.); martin.dornheim@hereon.de (M.D.)

Abstract: With the aim to find suitable hydrogen storage materials for stationary and mobile applications, multi-cation amide-based systems have attracted considerable attention, due to their unique hydrogenation kinetics. In this work, $A_mZn(NH_2)_n$ (with A = Li, K, Na, and Rb) were synthesized via an ammonothermal method. The synthesized phases were mixed via ball milling with LiH to form the systems $A_mZn(NH_2)_n$-$2n$LiH (with m = 2, 4 and n = 4, 6), as well as $Na_2Zn(NH_2)_4·0.5NH_3$-8LiH. The hydrogen storage properties of the obtained materials were investigated via a combination of calorimetric, spectroscopic, and diffraction methods. As a result of the performed analyses, $Rb_2Zn(NH_2)_4$-8LiH appears as the most appealing system. This composite, after de-hydrogenation, can be fully rehydrogenated within 30 s at a temperature between 190 °C and 200 °C under a pressure of 50 bar of hydrogen.

Keywords: energy; hydrogen storage; amides; *in-situ* X-ray diffraction; reaction mechanism

1. Introduction

Hydrogen is a renewable and environmentally friendly energy carrier, regarded as a potential candidate for supporting the epochal transition from fossil to renewable energy sources. Compared to common fossil fuels such as methane, diesel, etc., hydrogen possesses a higher gravimetric energy density [1]. However, under ambient conditions, its volumetric energy density is lower than fossil fuels. In order to increase this value, compression up to 750 bar, and liquefaction at cryogenic temperatures are commonly used methods. An additional method that enables achieving extremely high volumetric energy density is to store hydrogen in a solid-state using metal hydride and/or complex metal hydride-based systems. Compared to compression and liquefaction, solid-state storage allows operating the storage system at lower pressures (e.g., ≤100 bar) and without losses of hydrogen over time [2]. Due to their availability and high gravimetric and volumetric storage densities, metal hydrides such as magnesium and magnesium-based compounds were extensively explored as prospective hydrogen storage materials prior to the 2000 s [3–6]. However, in the present century, the scientific community's focus has been shifting to the development of sophisticated complex metal hydride-based hydrogen storage systems. Among the several

classes of these hydrides that are potentially suitable for hydrogen storage applications, in the last decade, amide-based systems have received increasing attention due to their high gravimetric and volumetric hydrogen capacities [7–12]. The first example of a fully reversible amide-based system for hydrogen storage applications was reported in 2002 by Chen et al. [13]. In this work, it was demonstrated that the system $LiNH_2$-2LiH could store reversibly about 9.5 wt.% of hydrogen.

The reversible exchange of hydrogen occurs through the following multistep reaction Equation (1):

$$LiNH_2 + 2LiH \rightleftharpoons Li_2NH + LiH + H_2 \rightleftharpoons Li_3N + 2H_2 \tag{1}$$
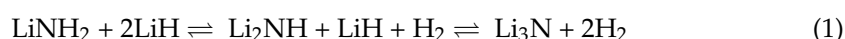
However, for the first step of the reaction, in spite of a calculated reaction enthalpy of $\Delta H \approx 45$ kJ/mol-H_2, a kinetic performance suitable for stationary and/or mobile applications can be achieved only at temperatures equal to or higher than 200 °C [13]. Thus, this system does not meet the performance criteria for operating in combination with proton exchange membrane (PEM) fuel cells. A considerable amount of work has been carried out in the last decade aiming at developing new amide-based systems for hydrogen storage applications. As a result of this scientific effort, several amide-hydride systems, possessing a wide range of thermodynamic and kinetic properties (e.g., Ca-N-H, Mg-N-H, Li-Mg-N-H, Li-Ca-N-H, Li-Al-N-H, Li-B-N-H), have been synthesized and their hydrogen storage properties have been tested [14–23]. For example, the replacement of $LiNH_2$ by $Mg(NH_2)_2$ and/or the substitution of 2LiH with MgH_2 in the $LiNH_2$-2LiH system led to the system $Mg(NH_2)_2$-2LiH/2$LiNH_2$-MgH_2 (2$LiNH_2$ + MgH_2 → $Li_2Mg(NH)_2$ + $2H_2 \rightleftharpoons Mg(NH_2)_2$ + 2LiH) [24–27], that possesses more favorable thermodynamic stability (i.e., $\Delta H \approx 40$ kJ/mol-H_2), whilst maintaining a high hydrogen storage capacity (5.6 wt.%) [28]. In addition, the use of selected additives/catalysts has been proven to be a successful strategy to improve the hydrogen storage performance of amide-hydride systems [29–40]. Transition metals such as Sc, Ti, V, Ta, Ni, and their compounds are known to be effective additives for improving the properties of amide-hydride systems [26,41–46]. Ichikawa et al. [42,43] first reported on the beneficial effect that the addition of nano-sized Ti additives entails on the $LiNH_2$-LiH system.

Zinc possesses chemical properties similar to those of nickel and titanium, which is known to be an effective additive for these systems, therefore the possibility to synthesize ternary amides containing alkali metals and zinc might be considered a good strategy to develop novel amide-based hydrogen storage systems with improved thermodynamic and kinetic properties. In this regard, previous works [47–49] on the systems $Li_4Zn(NH_2)_6$-12LiH and $K_2Zn(NH_2)_4$-8LiH showed extremely promising results, especially for the latter. In fact, the desorbed state of the system $K_2Zn(NH_2)_4$-8LiH can be fully rehydrogenated at ca. 230 °C within 30 s under a hydrogen pressure of 50 bar, whereas under the same conditions the de-hydrogenated state of $LiNH_2$-2LiH can absorb only a small amount of H_2. It must be mentioned that these excellent absorption properties are maintained upon cycling.

For the purpose of expanding the understanding of the de-hydrogenation/rehydrogenation mechanisms of zinc-containing ternary amides, the properties of the systems $Rb_2Zn(NH_2)_4$-8LiH and $Na_2Zn(NH_2)_4 \cdot 0.5NH_3$-8LiH are investigated and compared with those of the systems $LiNH_2$-2LiH, $Li_4Zn(NH_2)_6$-12LiH, and $K_2Zn(NH_2)_4$-8LiH.

2. Experimental Details

$A_mZn(NH_2)_n$ with m = 2, 4 and n = 4, 6 and A = Li, K, Na, and Rb were supplied by the University of Stuttgart [50,51]. These compounds were synthesized under supercritical ammonia in custom-built Alloy 718 (austenitic nickel—chromium—based superalloy) autoclaves. $Li_4Zn(NH_2)_6$ was grown in the cold temperature zone of the autoclave under ammonothermal conditions of 500 °C (furnace temperature) and 110 bar from zinc and lithium (molar metal ratio 1:4) in supercritical ammonia. $K_2Zn(NH_2)_4$, $Rb_2Zn(NH_2)_4$, and $Na_2Zn(NH_2)_4 \cdot 0.5NH_3$ were obtained in the cold temperature zone of the autoclave from zinc powder and KNH_2/$RbNH_2$/$NaNH_2$ (molar metal ratio 1:2) under ammonothermal

conditions (300 °C furnace temperature, 150 bar). $LiNH_2$ (95% purity) and LiH (97% purity) were purchased from Strem and Alfa, respectively. $LiNH_2$-2LiH, $Li_4Zn(NH_2)_6$-12LiH, $Na_2Zn(NH_2)_4 \cdot 0.5NH_3$-8LiH, $K_2Zn(NH_2)_4$-8LiH, and $Rb_2Zn(NH_2)_4$-8LiH are hereafter named as LH, LZH, NZH, KZH, and RZH, respectively. All the samples were ball-milled for 12 h at a milling regime of 250 rpm using a Fritsch Pulverisette 6 classic line planetary mill, with a ball to powder ratio of ca. 40:1 in a custom-made high-pressure vial under 50 bar of hydrogen. To prevent any possible contamination from atmospheric agents, the powder handling and milling were performed in an MBraun glovebox, in a continuously purified argon atmosphere (H_2O and O_2 levels below 1 ppm).

Differential thermal analyses (DTA), and mass spectroscopy (MS) analyses were carried out using a Netzsch STA 409 C instrument, coupled with a Hiden Analytical HAL 201 mass spectrometer. The samples were investigated upon heating in the temperature range of 20–500 °C, using a heating rate of 5 °C/min. Each measurement was carried out under an argon flow of 50 mL/min. For the MS characterization of the gaseous species, the evolution of H_2 (m/z = 2) and NH_3 (m/z = 17) was monitored. Considering that the purity of hydrogen is a key requirement for PEM fuel cells and that even the presence of a few ppm of NH_3 has a detrimental effect on their performance,[52,53] this characterization aims to understand if upon heating, only hydrogen is released from the investigated materials or if traces of ammonia are also present. It must be noted, however, that the release of extremely small amounts of NH_3 along with H_2 could be easily sequestered using targeted hydrides and/or ammonia adsorbents.

De-/rehydrogenation experiments were performed using a Sievert's type apparatus (Hera, QC J4G 1A1, Canada). In this machine, the values of desorbed and absorbed hydrogen are evaluated based on the differential pressure method, i.e., two holders of equal volume, one containing the investigated sample and the other empty, are connected by a differential pressure gauge. Upon heating and cooling, the temperature-induced pressure changes on the two sides of the gauge compensate for each other, whereas pressure differences due to desorption/absorption processes are recorded. The hydrogen absorption experiments were carried out in dynamic temperature conditions, heating the specimens from room temperature (RT) up to the final temperature of 300 °C using a heating rate of 3 °C/min, under a hydrogen pressure of 50 bar. The hydrogen desorption experiments were also carried out in dynamic temperature conditions, with the specimens heated from RT to 400 °C at a rate of 3 °C/min under static vacuum. Isothermal de-/rehydrogenation experiments were performed using the same Sievert's type apparatus at temperatures of 192 °C and 222 °C, in static vacuum (starting pressure of 10^{-2} bar) and 50 bar of hydrogen, respectively. The decisions to perform the de-hydrogenation measurement under static vacuum conditions and the hydrogenation reaction at 50 bar were taken to increase the likelihood of NH_3 release and to match the hydrogen pressure that is provided by a state-of-the-art commercial electrolyzer.

In-situ Synchrotron Radiation Powder X-ray Diffraction (*in-situ* SR-PXD) experiments were performed at the PETRA III Synchrotron facility at DESY beamline P.02.1, Germany. The X-ray wavelength (λ) utilized was fixed at 0.20745 Å and a Perkin Elmer plate image detector (2048 × 2048 pixels, each of size 200 × 200 μm^2) was used to acquire the 2D patterns, with a sample-to-detector distance of 1403 mm. Within an argon-filled glovebox GP (Campus) from Jacomex (H_2O and O_2 levels below 1 ppm), the samples were loaded into sapphire capillaries and then placed into a custom-designed sample cell, which allows controlling the temperatures and applying gases. SR-PXD experiments of the de-hydrogenation processes were performed by heating the specimens from RT to 350 °C, with a heating rate of 3 °C/min, under a static vacuum environment (starting pressure of 10^{-2} bar). SR-PXD experiments on the rehydrogenation processes were performed by heating the samples from RT to 300 °C with a heating rate of 10 °C/min, under an atmosphere of 50 bar of H_2. The software FIT2D was used to convert the acquired 2D images into 1D files.

Ex-situ PXD experiments were performed with a Bruker D8 Discover diffractometer from Bruker AXS GmbH, which was equipped with a copper X-ray source (Cu K radiation,

λ = 1.54184 Å) and a VANTEC–500 area detector. The diffraction patterns were acquired in steps of 15° (2θ) with an exposure time per step of 400° s under rotation conditions (1 rotation/min). In order to avoid detrimental oxidation phenomena, prior to performing the PXD investigation, the investigated specimens were loaded under an argon atmosphere into an especially designed polymethyl methacrylate (PMMA) airtight sample holder.

Although a comprehensive examination of the microstructural features of the researched materials is theoretically achievable using Rietveld refinement or the Debye Scherrer equation, this paper focuses on the refinement of only a few diffraction patterns made with the MAUD software [54–56].

3. Results and Discussion

As previously stated, the operating temperature and purity of the released hydrogen are crucial factors to consider when choosing the right material for a storage system that will work in conjunction with a PEM fuel cell (even if only as an additive). Aiming at investigating the thermal stability of the prepared materials and the purity of the released hydrogen, the coupled DTA-MS analyses of the ball-milled LH, LZH, NZH, KZH, and RZH were carried out, and the results are summarized in Figure 1. The DTA de-hydrogenation trace of LH shows the presence of a single endothermic signal having an onset temperature of about 160 °C and a maximum peak temperature of about 250 °C. The associated MS analysis indicates that during the decomposition of LH only hydrogen is released. In contrast to the LH system, the DTA traces of the other materials indicate the occurrence of the decomposition over several steps. For the LZH system, the first small and exothermic signal is visible, having an onset temperature of 70 °C, and it is accompanied by the release of a small amount of hydrogen. This event is followed by a broad endothermic signal, with an onset temperature of about 160 °C. For this signal, it is difficult to assign a unique value for the peak maximum, as it appears to be composed of overlapping endothermic events having peak maxima at about 210 °C, 240 °C, 280 °C, and 315 °C, respectively. Associated with these events, the release of pure hydrogen is observed. The DTA trace of the NZH system shows the presence of a broad endothermic signal having a temperature of about 160 °C, which can be separated into three different signals having peak maxima of about 205 °C, 240 °C, and 260 °C, respectively. This main event is followed by an additional endothermic signal having a peak maximum of 365 °C. The MS analysis of the gaseous phases released during the decomposition of NZH indicates that the release of hydrogen occurs in three main events having signal maxima of 205 °C, 365 °C, and 425 °C. Interestingly, this hydrogen desorption is accompanied by the release of small quantities of NH_3 in the range between 160 °C and 240 °C. The amount of released NH_3 increases significantly above 240 °C, reaching a maximum at 290 °C, before decreasing monotonically. The DTA trace of KZH shows the presence of two main endothermic signals. In addition, a small endothermic signal precedes the second main event. The first signal has an onset temperature of 160 °C and a peak maximum of 240 °C, whereas the second signal has an onset temperature of about 305 °C and a peak maximum of 365 °C. Both signals are associated with the release of hydrogen only. The DTA trace of the system RZH shows the presence of four main endothermic signals, having onset temperatures of 160 °C, m, 290 °C, and 350 °C, whereas the peak maxima are 240 °C, 270 °C, 315 °C, and 430 °C, respectively. The MS traces measured for the RZH system indicate that the system decomposes releasing only hydrogen. It must be noticed that the release of hydrogen associated with the endothermic signal at 350 °C is relatively small if compared with the DTA signal. This DTA peak is most likely connected with the sublimation of a fraction of the sample.
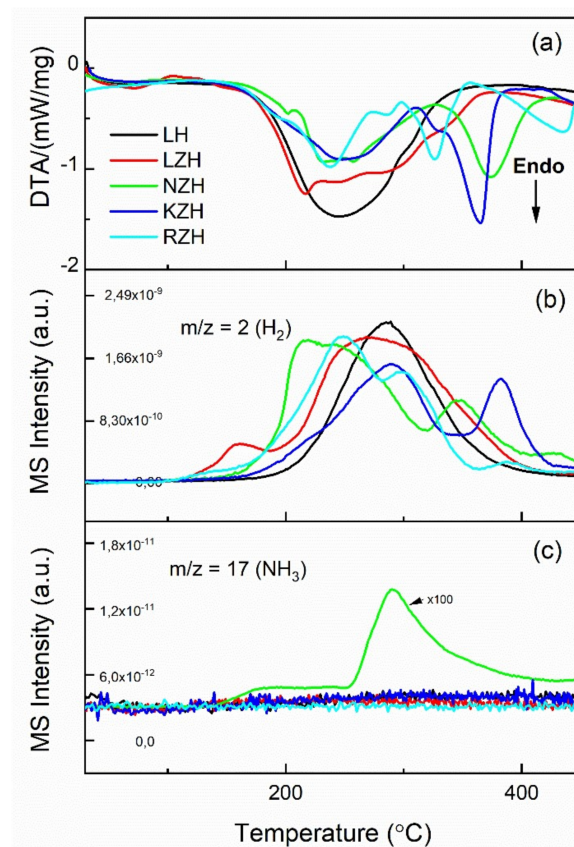
Figure 1. DTA-MS analyses of LZH, NZH, KZH, RZH, and the reference LH, respectively. DTA curves (**a**), H_2 MS spectra (**b**) and NH_3 MS spectra (**c**). All the samples were heated from RT to 500 °C under 50 mL/min of argon flow with a heating rate of 5 °C/min.

In order to shed further light on the hydrogen storage properties of the investigated systems, the kinetics of the first de-hydrogenation/rehydrogenation cycle was characterized by means of volumetric technique. The results of this investigation are displayed in Figure 2. Upon heating, the LH system starts to release hydrogen at about 160 °C, however, significant quantities of hydrogen are released only at temperatures higher than 200 °C. The overall de-hydrogenation process occurs in a single step and the final amount of released hydrogen at 390 °C is 4.2 wt.%. As previously observed in the coupled DTA-MS analyses, the hydrogen release from the system LZH starts at around 100 °C and increases considerably at temperatures higher than 180 °C, reaching a value of 5.3 wt.% at 390 °C. The system NZH, similarly to LH, starts to desorb hydrogen at around 160 °C. As observed in the DTA analysis of Figure 1, the decomposition reaction appears to occur in two separate steps. The measured amount of released hydrogen at 390 °C (i.e., 4.8 wt.%) is slightly overestimated, due to the simultaneous release of NH_3. The de-hydrogenation reaction of KZH starts at about 160 °C and, through a three steps kinetics, reaches a final amount of released hydrogen of 3.9 wt.% at 390 °C. The de-hydrogenation reaction of the system RZH starts at about 160 °C and, in two-step kinetics, reaches a maximum amount of desorbed hydrogen equal to 3.2 wt.% at 390 °C.
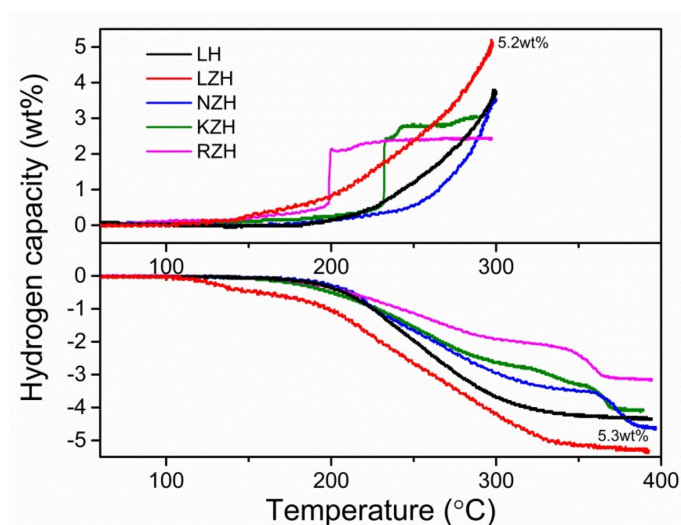
Figure 2. Volumetric hydrogen release and absorption curves of LZH, NZH, KZH, RZH, and LH samples: hydrogen desorption from RT to 400 °C with a heating rate of 3 °C/min under static vacuum (bottom graph); hydrogen absorption from RT to 300 °C with a heating rate of 3 °C/min under 50 bar of H_2 (top graph).

The de-hydrogenated materials were subsequently rehydrogenated under dynamic conditions in the temperature range between RT and 300 °C. Upon heating, the LZH system starts to absorb hydrogen already at 140 °C, reaching a final H_2 amount equal to 5.2 wt.%, while the LH system starts to absorb hydrogen at about 180 °C, and the maximum amount is equal to 4.0 wt.% at 300 °C. The NZH system starts to absorb hydrogen at 180 °C and, in two steps, reaches a final amount equal to 3.8 wt.%. The hydrogen absorption of the KZH system starts at about 140 °C. As already reported in ref. [48], the hydrogen absorption of this system is characterized by the presence of an extremely fast absorption step occurring at about 230 °C. In this step, within less than a minute, more than 50% of the overall hydrogen is absorbed. A final absorption step between 230 °C and 300 °C resulted in an overall capacity of 3.0 wt.%. The RZH system starts to absorb small quantities of hydrogen already at temperatures lower than 100 °C. A sensible increase of the hydrogenation rate is observed at about 140 °C, leading to a total hydrogen capacity of about 0.6 wt.% at 190 °C. Interestingly, this system, like KZH, shows an extremely fast absorption step. At 195 °C, the material absorbs more than half of the total capacity (i.e., 1.4 wt.%) in less than a minute. A final absorption step at temperatures ranging from 210 to 300 °C results in a final hydrogen storage capacity of 2.6 wt.%.

Among the investigated materials, the KZH and RZH systems are the only ones that show an extremely fast hydrogen uptake at a well-defined temperature. Considering that the properties and reaction mechanism of KZH were already partially studied in a previous publication [47], the focus of the present work will be on the RZH system. The results obtained by the volumetric investigation of the first three de-hydrogenation/rehydrogenation cycles of the system RZH are reported in Figure 3. The second and third de-hydrogenation/rehydrogenation cycles present similar features. The de-hydrogenation occurs always in two consecutive steps that lead to a final amount of released hydrogen of about 2.8 wt.%. The de-hydrogenation onset temperature for the first step shifts (to 180 °C and 225 °C for the second and third cycles, respectively). The second and third rehydrogenation cycles trace out the first one in the range of temperatures between RT and 190 °C. However, the fast hydrogenation step, although leading to the same amount of stored hydrogen, is shifted to higher temperatures, i.e., about 210 °C, and appears to result from two different hydrogenation events, closely following one another. As observed also for the de-hydrogenation measurement, the final hydrogen storage capacity of the material remains about 2.6 wt.%.
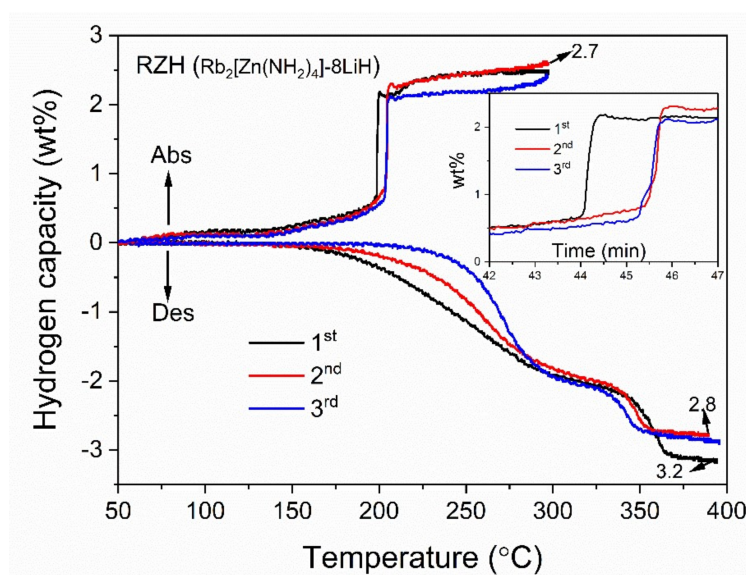
Figure 3. Volumetric analysis of the first three de-/rehydrogenation cycles of RZH carried out under static vacuum (initial pressure value 10^{-2} bar) and 50 bar of H_2, respectively. The material was heated from RT up to 400 °C for the de-hydrogenation measurement, whereas for the rehydrogenation measurement was heated from RT up to 300 °C. The used heating rate was 3 °C/min, in both cases.

The de-hydrogenation reaction of the RZH system was further characterized by *in-situ* SR-PXD measurements. The results of this investigation are shown in Figure 4. The ball-milled RZH powders are composed of $LiNH_2$, LiH, and Rb_2ZnH_4. Upon heating at ca. 310 °C, the diffraction peaks of Rb_3ZnH_5 appear along with those of Li_2NH and $Li_{0.105}Zn_{0.985}$; finally, at 340 °C, only the signals of Li_2NH and $Li_{0.105}Zn_{0.985}$ are visible. Unexpectedly, no diffraction peaks related to Rb containing phases were observed even during the cooling period. In a previous work on the de-hydrogenation mechanism of KZH, *in-situ* SR-PXD showed the formation of KH [47]. Figure 3 indicates that the hydrogen storage properties and reaction mechanisms of KZH and RZH are similar [47,57]. Thus, the formation of phases such as RbH, Rb-based alloys, or Rb (depending on the applied hydrogen backpressure) during the de-hydrogenation of RZH is expected.
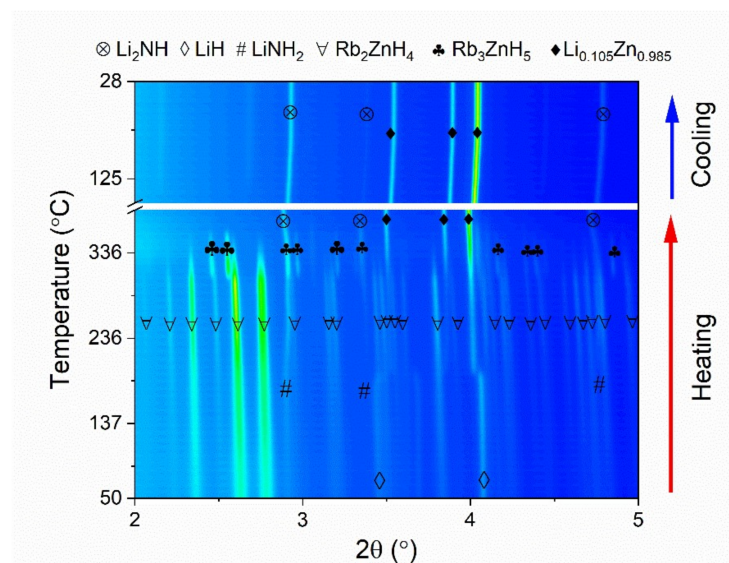
Figure 4. *In-situ* SR-PXD analysis of the de-hydrogenation process of the system RZH. The measurement was carried out heating the material from RT to 350 °C with a heating rate of 3 °C/min under dynamic vacuum (pressure value 10^{-2} mbar). Utilized X-ray wavelength (λ) = 0.20745 Å.

Aiming at probing this eventuality, following the experimental conditions applied for the *in-situ* analysis of Figure 4, a small batch of RHZ was de-hydrogenated in a Sievert's type apparatus and the product characterized by XRD (Figure 5).
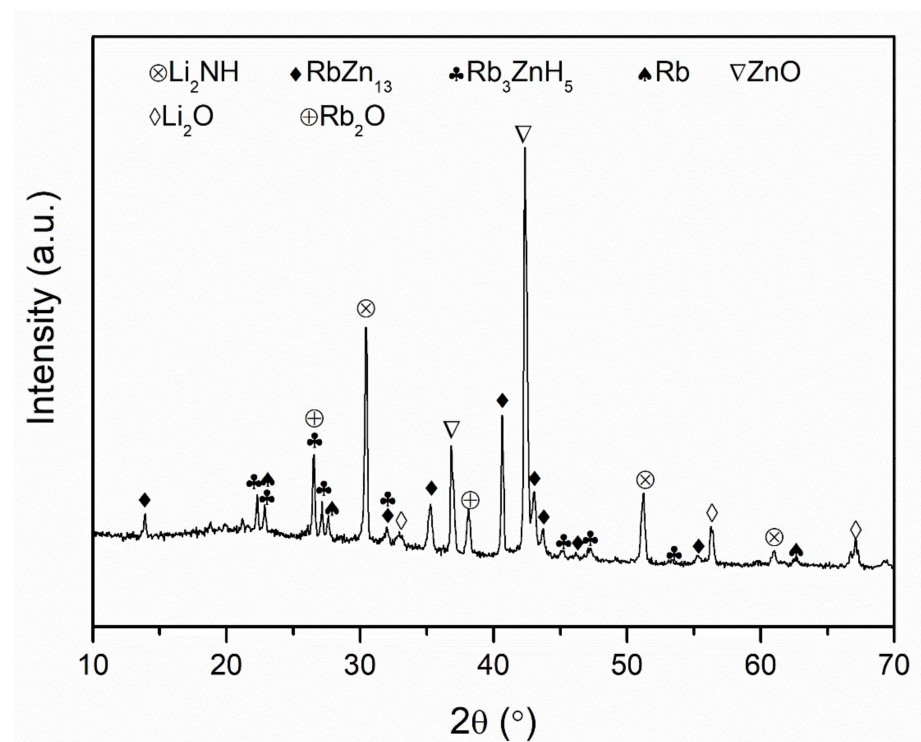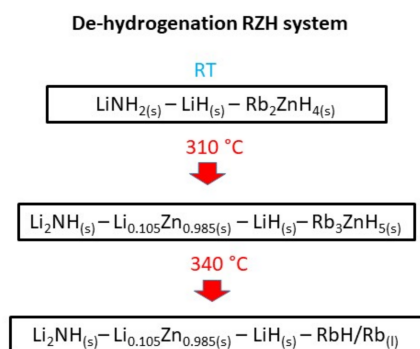

Figure 5. *Ex-situ* PXD analysis of the de-hydrogenated RZH system. The measurement was carried out utilizing an X-ray wavelength (λ) = 1.54184 Å.

The presence of diffraction peaks ascribable to Rb, $RbZn_{13}$, and $RbZnH_5$ in the diffraction patterns of the de-hydrogenated sample confirms the previously mentioned supposition. In addition, the presence of Li_2NH, ZnO, Li_2O, and Rb_2O is also observed. The absence of any diffraction peak related to Rb containing phases in the cooling part of the SR-PXD analysis of Figure 4 is most likely due to their displacement (segregation), with respect to the X-ray beam position. Indeed, because the capillary of the SR-PXD cell is exposed to a significant temperature gradient between the central area (the area hit by the X-ray beam) and the peripheral areas (the areas of the connection between the capillary and the cell), molten phases can move to the colder areas of the capillary. This eventuality is supported by a picture of the capillary taken after the de-hydrogenation measurement and reported in Figure A1, where it is possible to notice the presence of a phase of shiny metallic grey color (presumably metallic Rb) at the extreme left of the capillary, next to the position where the sample was located at the beginning of the measurement (a part of the sample still occupies this area).

Based on the SR-PXD analysis of Figure 4 and the above discussion, a possible reaction scheme for the de-hydrogenation process can be envisaged as depicted in Figure 6.

Due to the displacement of a portion of the sample under operating conditions (Figure A1), the *in-situ* SR-PXD analysis of the rehydrogenation process was not attempted. Instead, the PXD analysis of the RZH system after the third rehydrogenation cycle was carried out and the obtained diffraction pattern was analyzed by Rietveld's method (Figure 7). As for the as-milled material (Figure 4), the crystalline phases composing the RZH system cycled three times are $LiNH_2$, LiH, and Rb_2ZnH_4 in the amounts of 26.9 wt.%, 11.9 wt.%, and 61.2 wt.%, respectively. Thus, as suggested by the volumetric analysis of Figure 3, the result of this PXD analysis confirms that the RZH system is fully reversible.
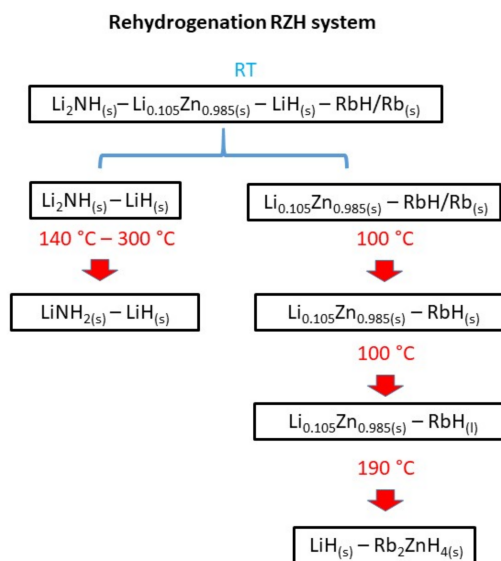
Figure 6. Proposed de-hydrogenation mechanism of the RZH system for the range of temperature RT—350 °C.
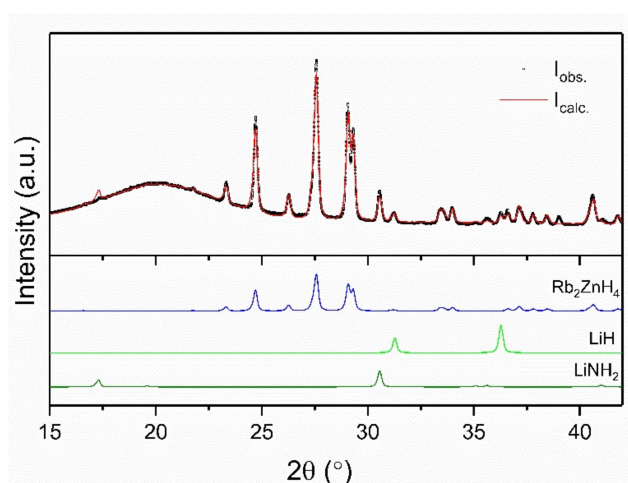
Figure 7. *Ex-situ* PXD analysis of the system RZH after the third rehydrogenation cycle. The measurement was carried out utilizing an X-ray wavelength (λ) = 1.54184 Å.

Even though no *in-situ* SR-PXD analysis is available on the rehydrogenation process of the RZH system, some speculations on the reaction mechanism can be made. The hydrogenation step, starting at about 100 °C, can be attributed to the hydrogenation of the Rb formed during the de-hydrogenation process. Then, considering that after this initial hydrogenation step, the system is composed most likely of Li_2NH, $Li_{0.105}Zn_{0.985}$, LiH, and RbH/Rb, whereas the hydrogenation products are $LiNH_2$, LiH, and Rb_2ZnH_4, the rehydrogenation process can be divided into two sub-processes: (1) the hydrogenation of Li_2NH to form $LiNH_2$—LiH (similarly to the system LH) and (2) the hydrogenation of $Li_{0.105}Zn_{0.985}$—RbH/Rb to form Rb_2ZnH_4—LiH. Observing the hydrogenation kinetics of the system LH (Figure 2), it is clear that the reaction occurs in a single step, which leads to reaching the system's final hydrogen storage capacity monotonously. Thus, it is unlikely that this sub-process is the one responsible for the fast hydrogenation behavior observed in the RZH system. In the opinion here advocated, it is more likely that this peculiar behavior is due to the hydrogenation of solid $Li_{0.105}Zn_{0.985}$ and molten RbH/Rb (RbH melting point = 170 °C) to form Rb_2ZnH_4 and LiH. The observation that this extremely quick phenomenon occurs in two different steps (visible in the 2nd and 3rd rehydrogenation cycles of the insert in Figure 3) might be justified by a possible inhomogeneous phase distribution in the cycled RZH system. Based on these assumptions, a possible reaction scheme for the rehydrogenation process can be envisaged as depicted in Figure 8.

Rehydrogenation RZH system

Figure 8. Proposed rehydrogenation mechanism of the RZH system for the range of temperature RT—300 °C.

The extremely fast kinetics of the formation of ternary transition metal hydrides, such as Rb_2ZnH_4, combined with their high degree of reversibility, makes them appear as extremely interesting compounds for hydrogen storage purposes. Unfortunately, their hydrogen storage capacity is insufficient to qualify them for use as hydrogen storage materials. For instance, despite the fact that their gravimetric capacity is comparable to that of compounds with a high potential for commercial use (e.g., TiFe [58,59], $Ti_{0.95}Zr_{0.05}Mn_{1.46}V_{0.45}Fe_{0.09}$ [60], etc.), their operational temperature is too high. However, because of the high catalytic activity that transition metal-based elements have on metal amide-based systems [53], $A_mZn(NH_2)_n$ could play an important role in the development of novel hydrogen storage materials with enhanced kinetic properties. In this regard, the beneficial effect of an $A_mZn(NH_2)_n$ compound on the hydrogen storage properties of the amide system $2LiH-Mg(NH_2)_2$ has recently been demonstrated, and the mechanism of action has been partially explained [54]. One might object that the operating temperatures of the species responsible for the fast hydrogenation kinetics of the system studied in this work are still too high for the expected range of operation of a hydride-based system, which is supposed to work in combination with a PEM fuel cell. However, when it comes to the use of additive compounds similar to Rb_2ZnH_4 for improving the hydrogen storage properties of amide-based systems, $ZrCoH_3$ is one of the most effective additives ever reported for the system $2LiNH_2+1.1MgH_2+0.1LiBH_4$ [55–59] In fact, by adding 3 wt.% $ZrCoH_3$, once desorbed, it is possible to store about 5.3 wt.% of hydrogen in 10 min at 150 °C and a hydrogen atmosphere of 70 bar, whereas at the same temperature, it is possible to desorb 3.8 wt.% of hydrogen in 60 min under 1 bar of hydrogen pressure. Under these operating conditions, the chemical environments of both Zr and Co atoms, as well as the crystal properties of $ZrCoH_3$, appear to be unaltered during de-/rehydrogenation processes [56].

4. Conclusions

Ternary amides, containing alkali and transition metals, appear to be appealing compounds for the development of hydrogen storage systems. In previous works and in this manuscript, several different systems were synthesized and their hydrogen storage properties were investigated. Among them, $K_2Zn(NH_2)_4$-8LiH, $K_2Mn(NH_2)_4$-8LiH, and $Rb_2Zn(NH_2)_4$-8LiH display unique rehydrogenation features. In fact, the desorption products of these systems can reabsorb most of the released hydrogen within a short time frame. At 230 °C and 50 bar of hydrogen pressure, $K_2Zn(NH_2)_4$-8LiH fully rehydrogenates in 30 s,

with a maximum hydrogenation rate of 6 wt.%/min. At 230 °C and 50 bar of hydrogen pressure, $K_2Mn(NH_2)_4$-8LiH fully rehydrogenates in 30 s, with a maximum hydrogenation rate of 3 wt.%/min. In this manuscript, it has been demonstrated that under a hydrogen pressure of 50 bar, $Rb_2Zn(NH_2)_4$-8LiH can reabsorb the majority of the released hydrogen between 190 and 200 °C in 30 s, reaching a maximum hydrogenation rate of 3 wt.%/min. For the other investigated systems, re-hydrogenation is slower and not fully reversible. Concerning desorption, the Rb system starts to release pure hydrogen at 160°C and the reaction evolves in two steps. In the Na system, the hydrogen release starts at the same temperature, but some ammonia is released during the evolution of the process. Despite these unique hydrogen storage features, the use in commercial hydrogen storage applications of these systems is hampered by the fact that they do not meet the target requirements for working in combination with PEM fuel cells.

Author Contributions: Conceptualization, C.P. and H.C.; formal analysis, C.P., H.C. and C.M.; investigation, H.C., T.M.M.R., G.C., J.-C.T. and Y.S.; resources, C.M., R.N., P.C. and M.D.; writing—original draft preparation, C.P. and H.C.; writing—review and editing, C.M., G.C., R.N., P.C., T.K. and M.D.; supervision, C.P. All authors have read and agreed to the published version of the manuscript.

Data Availability Statement: The data presented in this study are available on request from the corresponding author.

Conflicts of Interest: The authors declare no conflict of interest.

Appendix A
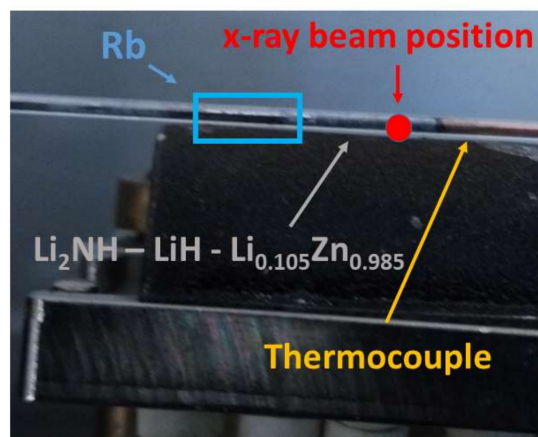
Figure A1. Picture of the SR-PXD cell, taken after the 1st de-hydrogenation measurement of the RZH system.

References

1. Schlapbach, L.; Zuttel, A. Hydrogen-storage materials for mobile applications. *Nature* **2001**, *414*, 353–358. [CrossRef] [PubMed]
2. Pistidda, C. Solid-State Hydrogen Storage for a Decarbonized Society. *Hydrogen* **2021**, *2*, 428–443. [CrossRef]
3. Gautam, Y.K.; Chawla, A.K.; Khan, S.A.; Agrawal, R.; Chandra, R. Hydrogen absorption and optical properties of Pd/Mg thin films prepared by DC magnetron sputtering. *Int. J. Hydrogen Energy* **2012**, *37*, 3772–3778. [CrossRef]
4. Gautam, Y.K.; Chawla, A.K.; Walia, R.; Agrawal, R.; Chandra, R. Hydrogenation of Pd-capped Mg thin films prepared by DC magnetron sputtering. *Appl. Surf. Sci.* **2011**, *257*, 6291–6295. [CrossRef]
5. Gautam, Y.K.; Kumar, M.; Chandra, R. Hydrogen absorption and desorption properties of Pd/Mg/Pd tri-layers prepared by magnetron sputtering. *Surf. Coatings Technol.* **2013**, *237*, 450–455. [CrossRef]
6. Shang, Y.; Pistidda, C.; Gizer, G.; Klassen, T.; Dornheim, M. Mg-based materials for hydrogen storage. *J. Magnes. Alloy.* **2021**. [CrossRef]

7. He, T.; Cao, H.; Chen, P. Complex Hydrides for Energy Storage, Conversion, and Utilization. *Adv. Mater.* **2019**, *31*, e1902757. [CrossRef] [PubMed]
8. He, T.; Pachfule, P.; Wu, H.; Xu, Q.; Chen, P. Hydrogen carriers. *Nat. Rev. Materials.* **2016**, *1*, 1–17.
9. Milanese, C.; Jensen, T.R.; Hauback, B.; Pistidda, C.; Dornheim, M.; Yang, H.; Lombardo, L.; Zuettel, A.; Filinchuk, Y.; Ngene, P.; et al. Complex hydrides for energy storage. *Int. J. Hydrogen Energy* **2019**, *44*, 7860–7874. [CrossRef]
10. Orimo, S.I.; Nakamori, Y.; Eliseo, J.R.; Zuttel, A.; Jensen, C.M. Complex hydrides for hydrogen storage. *Chem. Reviews.* **2007**, *107*, 4111–4132. [CrossRef]
11. Eghbali, P.; Nişancı, B.; Metin, Ö. Graphene hydrogel supported palladium nanoparticles as an efficient and reusable heterogeneous catalysts in the transfer hydrogenation of nitroarenes using ammonia borane as a hydrogen source. *Pure Appl. Chem.* **2018**, *90*, 327–335. [CrossRef]
12. Eghbali, P.; Gürbüz, M.U.; Ertürk, A.S.; Metin, Ö. In situ synthesis of dendrimer-encapsulated palladium(0) nanoparticles as catalysts for hydrogen production from the methanolysis of ammonia borane. *Int. J. Hydrogen Energy* **2020**, *45*, 26274–26285. [CrossRef]
13. Chen, P.; Xiong, Z.; Luo, J.; Lin, J.; Tan, K.L. Interaction of hydrogen with metal nitrides and imides. *Nature* **2002**, *420*, 302–304. [CrossRef] [PubMed]
14. Baricco, M.; Bang, M.; Fichtner, M.; Hauback, B.; Linder, M.; Luetto, C.; Moretto, P.; Sgroi, M. SSH2S: Hydrogen storage in complex hydrides for an auxiliary power unit based on high temperature proton exchange membrane fuel cells. *J. Power Sources* **2017**, *342*, 853–860. [CrossRef]
15. Cui, J.R.; Zhang, W.J.; Cao, H.J.; Chen, P. Mild-condition synthesis of A(2)ZnH(4) (A = K, Rb, Cs) and their effects on the hydrogen storage properties of 2LiH-Mg(NH2)(2). *J. Energy Chemistry.* **2020**, *50*, 358–364. [CrossRef]
16. Garroni, S.; Santoru, A.; Cao, H.; Dornheim, M.; Klassen, T.; Milanese, C.; Gennari, F.; Pistidda, C. Recent Progress and New Perspectives on Metal Amide and Imide Systems for Solid-State Hydrogen Storage. *Energies* **2018**, *11*, 1027. [CrossRef]
17. Hu, J.; Fichtner, M.; Baricco, M. Preparation of Li-Mg-N-H hydrogen storage materials for an auxiliary power unit. *Int. J. Hydrogen Energy* **2017**, *42*, 17144–17148. [CrossRef]
18. Hu, J.; Wu, G.; Liu, Y.; Xiong, A.Z.; Chen, P.; Murata, K.; Sakata, K.; Wolf, G. Hydrogen Release from Mg(NH2)2−MgH2 through Mechanochemical Reaction. *J. Phys. Chem. B* **2006**, *110*, 14688–14692. [CrossRef]
19. Li, C.; Li, C.; Fan, M.; Chen, H.; Shu, K.; Zhang, Y.; Gao, M.; Liu, Y.; Pan, H. Synthesis of a ternary amide LixKy(NH2)(x+y) and a novel Li3K(NH2)(4)-xMgH(2) combination system for hydrogen storage. *J. Energy Chemistry.* **2019**, *35*, 37–43. [CrossRef]
20. Lin, H.-J.; Li, H.-W.; Murakami, H.; Akiba, E. Remarkably improved hydrogen storage properties of LiNH2-LiH composite via the addition of CeF4. *J. Alloy. Compd.* **2018**, *735*, 1017–1022. [CrossRef]
21. Zhang, Z.; Cao, H.; Zhang, W.; Cui, J.; Xiong, Z.; Chen, P. Thermochemical transformation and reversible performance of Mg(NH2)2–NaMgH3 system. *Int. J. Hydrogen Energy* **2020**, *45*, 23069–23075. [CrossRef]
22. Albanesi, L.F.; Garroni, S.; Larochette, P.A.; Nolis, P.; Mulas, G.; Enzo, S.; Baró, M.D.; Gennari, F.C. Role of aluminum chloride on the reversible hydrogen storage properties of the Li–N–H system. *Int. J. Hydrog. Energy.* **2015**, *40*, 13506–13517. [CrossRef]
23. Wu, G.; Xiong, Z.; Liu, T.; Liu, Y.; Hu, J.; Chen, P.; Feng, Y.; Wee, A.T. Synthesis and Characterization of a New Ternary ImideLi2Ca(NH)2. *Inorg. Chem.* **2007**, *46*, 517–521. [CrossRef] [PubMed]
24. Leng, H.Y.; Ichikawa, T.; Isobe, S.; Hino, S.; Hanada, N.; Fujii, H. Desorption behaviours from metal-N-H systems synthesized by ball milling. *J. Alloy. Compounds.* **2005**, *404*, 443–447. [CrossRef]
25. Luo, W. (LiNH2–MgH2): A viable hydrogen storage system. *J. Alloy. Compd.* **2004**, *381*, 284–287. [CrossRef]
26. Nakamori, Y.; Kitahara, G.; Miwa, K.; Ohba, N.; Noritake, T.; Towata, S.; Orimo, S. Hydrogen storage properties of Li-Mg-N-H systems. *J. Alloy. Compounds.* **2005**, *404*, 396–398. [CrossRef]
27. Xiong, Z.; Wu, G.; Hu, J.; Chen, P. Ternary Imides for Hydrogen Storage. *Adv. Mater.* **2004**, *16*, 1522–1525. [CrossRef]
28. Xiong, Z.; Hu, J.; Wu, G.; Chen, P.; Luo, W.; Gross, K.; Wang, J. Thermodynamic and kinetic investigations of the hydrogen storage in the Li-Mg-N-H system. *J. Alloy. Compounds.* **2005**, *398*, 235–239. [CrossRef]
29. Cao, H.; Pistidda, C.; Riglos, M.V.C.; Chaudhary, A.-L.; Capurso, G.; Tseng, J.-C.; Puszkiel, J.; Wharmby, M.T.; Gemming, T.; Chen, P.; et al. Conversion of magnesium waste into a complex magnesium hydride system: Mg(NH2)2–LiH. *Sustain. Energy Fuels* **2020**, *4*, 1915–1923. [CrossRef]
30. Durojaiye, T.; Hayes, J.; Goudy, A. Potassium, rubidium and cesium hydrides as dehydrogenation catalysts for the lithium amide/magnesium hydride system. *Int. J. Hydrogen Energy* **2015**, *40*, 2266–2273. [CrossRef]
31. Gizer, G.; Puszkiel, J.; Cao, H.; Pistidda, C.; Le, T.T.; Dornheim, M.; Klassen, T. Tuning the reaction mechanism and hydrogenation/dehydrogenation properties of 6Mg(NH2)29LiH system by adding LiBH4. *Int. J. Hydrogen Energy* **2019**, *44*, 11920–11929. [CrossRef]
32. Liu, Y.; Li, C.; Li, B.; Gao, M.; Pan, H. Metathesis Reaction-Induced Significant Improvement in Hydrogen Storage Properties of the KF-Added Mg(NH2)2–2LiH System. *J. Phys. Chem. C* **2013**, *117*, 866–875. [CrossRef]
33. Miao, N.; Zhou, X.L.; Lin, X.; Shi, Y.; Leng, H.Y.; Li, Q. Effect of LiCe(BH4)(3)Cl with a high Li ion conductivity on the hydrogen storage properties of Li-Mg-N-H system. *Int. J. Hydrog. Energy.* **2019**, *44*, 29150–29158. [CrossRef]
34. Wang, H.; Wu, G.; Cao, H.; Pistidda, C.; Chaudhary, A.-L.; Garroni, S.; Dornheim, M.; Chen, P. Near Ambient Condition Hydrogen Storage in a Synergized Tricomponent Hydride System. *Adv. Energy Mater.* **2017**, *7*. [CrossRef]

35. Wang, J.; Liu, T.; Wu, G.; Li, W.; Liu, Y.; Araújo, C.M.; Scheicher, R.H.; Blomqvist, A.; Ahuja, R.; Xiong, Z.; et al. Potassium-Modified Mg(NH2)(2)/2 LiH System for Hydrogen Storage. *Angew. Chem. -Int. Edition.* **2009**, *48*, 5828–5832. [CrossRef] [PubMed]

36. Wood, B.C.; Stavila, V.; Poonyayant, N.; Heo, T.W.; Ray, K.G.; Klebanoff, L.E.; Udovic, T.J.; Lee, J.R.I.; Angboonpong, N.; Sugar, J.D.; et al. Hydrogen Storage: Nanointerface-Driven Reversible Hydrogen Storage in the Nanoconfined Li-N-H System (Adv. Mater. Interfaces 3/2017). *Adv. Mater. Interfaces* **2017**, *4*. [CrossRef]

37. Xia, G.; Li, D.; Chen, X.; Tan, Y.; Tang, Z.; Guo, Z.; Liu, H.; Liu, Z.; Yu, X. Carbon-Coated Li3N Nanofibers for Advanced Hydrogen Storage. *Adv. Mater.* **2013**, *25*, 6238–6244. [CrossRef]

38. Yan, M.-Y.; Sun, F.; Liu, X.-P.; Ye, J.-H.; Wang, S.-M.; Jiang, L.-J. Effects of graphite content and compaction pressure on hydrogen desorption properties of Mg(NH2)2–2LiH based tank. *J. Alloy. Compd.* **2015**, *628*, 63–67. [CrossRef]

39. Zhang, J.; Liu, Y.; Zhang, X.; Yang, Y.; Zhang, Q.; Jin, T.; Wang, Y.; Gao, M.; Sun, L.; Pan, H. Synthesis of CsH and its effect on the hydrogen storage properties of the Mg(NH2)2-2LiH system. *Int. J. Hydrogen Energy* **2016**, *41*, 11264–11274. [CrossRef]

40. Zhang, Y.; Liu, Y.; Yang, Y.; Li, Y.; Hu, J.; Gao, M.; Pan, H. Superior catalytic activity of in situ reduced metallic Co for hydrogen storage in a Co(OH)(2)-containing LiBH4/2LiNH(2) composite. *Mater. Res. Bulletin.* **2018**, *97*, 544–552. [CrossRef]

41. Gizer, G.; Cao, H.; Puszkiel, J.; Pistidda, C.; Santoru, A.; Zhang, W.; He, T.; Chen, P.; Klassen, T.; Dornheim, M. Enhancement Effect of Bimetallic Amide K2Mn(NH2)4 and In-Situ Formed KH and Mn4N on the Dehydrogenation/Hydrogenation Properties of Li–Mg–N–H System. *Energies* **2019**, *12*, 2779. [CrossRef]

42. Ichikawa, T.; Hanada, N.; Isobe, S.; Leng, H.Y.; Fujii, H. Hydrogen storage properties in Ti catalyzed Li-N-H system. *J. Alloy. Compounds.* **2005**, *404*, 435–438. [CrossRef]

43. Isobe, S.; Ichikawa, T.; Hanada, N.; Leng, H.; Fichtner, M.; Fuhr, O.; Fujii, H. Effect of Ti catalyst with different chemical form on Li–N–H hydrogen storage properties. *J. Alloy. Compd.* **2005**, *404–406*, 439–442. [CrossRef]

44. Nguyen, T.T.T.; Reed, D.; Book, D.; Anderson, P. Hydrogen release and uptake in the Li-Zn-N system. *J. Alloy. Compounds.* **2015**, *645*, S295–S298. [CrossRef]

45. Zhang, T.; Isobe, S.; Matsuo, M.; Orimo, S.-I.; Wang, Y.; Hashimoto, N.; Ohnuki, S. Effect of Lithium Ion Conduction on Hydrogen Desorption of LiNH2–LiH Solid Composite. *ACS Catal.* **2015**, *5*, 1552–1555. [CrossRef]

46. Zhang, W.; Wang, H.; Cao, H.; He, T.; Guo, J.; Wu, G.; Chen, P. Effects of doping FeCl 3 on hydrogen storage properties of Li-N-H system. *Prog. Nat. Sci.* **2017**, *27*, 139–143. [CrossRef]

47. Cao, H.; Pistidda, C.; Richter, T.M.M.; Santoru, A.; Milanese, C.; Garroni, S.; Bednarcik, J.; Chaudhary, A.-L.; Gizer, G.; Liermann, H.-P.; et al. In Situ X-ray Diffraction Studies on the De/rehydrogenation Processes of the K2[Zn(NH2)4]-8LiH System. *J. Phys. Chem. C* **2017**, *121*, 1546–1551. [CrossRef]

48. Cao, H.; Richter, T.M.M.; Pistidda, C.; Chaudhary, A.-L.; Santoru, A.; Gizer, G.; Niewa, R.; Chen, P.; Klassen, T.; Dornheim, M. Ternary Amides Containing Transition Metals for Hydrogen Storage: A Case Study with Alkali Metal Amidozincates. *ChemSusChem* **2015**, *8*, 3777–3782. [CrossRef]

49. Cao, H.; Santoru, A.; Pistidda, C.; Richter, T.M.M.; Chaudhary, A.-L.; Gizer, G.; Niewa, R.; Chen, P.; Klassen, T.; Dornheim, M. New synthesis route for ternary transition metal amides as well as ultrafast amide–hydride hydrogen storage materials. *Chem. Commun.* **2016**, *52*, 5100–5103. [CrossRef]

50. Richter, T.M.M.; Zhang, S.; Niewa, R. Ammonothermal synthesis of dimorphic K2[Zn(NH2)4]. *Z. Für Krist. - Cryst. Materials.* **2013**, *228*, 351–358. [CrossRef]

51. Richter, T.M.M.; Alt, N.S.A.; Schlücker, E.; Niewa, R. Ammonothermal Synthesis and Characterization of Li4[Zn(NH2)4](NH2)2. *Chemistry* **2015**, *641*, 1016–1023. [CrossRef]

52. Uribe, F.A.; Gottesfeld, S.; Zawodzinski, T.A., Jr. Effect of ammonia as potential fuel impurity on proton exchange membrane fuel cell performance. *J. Electrochem. Society.* **2002**, *149*, A293–A296. [CrossRef]

53. Soto, H.J.; Lee, W.-K.; Van Zee, J.W.; Murthy, M. Effect of Transient Ammonia Concentrations on PEMFC Performance. *Electrochem. Solid-State Lett.* **2003**, *6*, A133–A135. [CrossRef]

54. Lonardelli, I.; Wenk, H.-R.; Lutterotti, L.; Goodwin, M. Texture analysis from synchrotron diffraction images with the Rietveld method: Dinosaur tendon and salmon scale. *J. Synchrotron Radiat.* **2005**, *12*, 354–360. [CrossRef] [PubMed]

55. Lutterotti, L.; Bortolotti, M.; Ischia, G.; Lonardelli, I.; Wenk, H.R. Rietveld texture analysis from diffraction images. *Z. Fur Kristallographie* **2007**, *26*, 125–130. [CrossRef]

56. Ghanbari, F.; Hassani, A.; Wacławek, S.; Wang, Z.; Matyszczak, G.; Lin, K.-Y.A.; Dolatabadi, M. Insights into paracetamol degradation in aqueous solutions by ultrasound-assisted heterogeneous electro-Fenton process: Key operating parameters, mineralization and toxicity assessment. *Sep. Purif. Technol.* **2021**, *266*, 118533. [CrossRef]

57. Wang, H.; Cao, H.J.; Wu, G.T.; He, T.; Chen, P. The improved Hydrogen Storage Performances of the Multi-Component Composite: 2Mg(NH2)(2)-3LiH-LiBH4. *Energies* **2015**, *8*, 6898–6909. [CrossRef]

58. Dematteis, E.M.; Berti, N.; Cuevas, F.; Latroche, M.; Baricco, M. Substitutional effects in TiFe for hydrogen storage: A comprehensive review. *Mater. Adv.* **2021**, *2*, 2524–2560. [CrossRef]

59. Dematteis, E.M.; Dreistadt, D.M.; Capurso, G.; Jepsen, J.; Cuevas, F.; Latroche, M. Fundamental hydrogen storage properties of TiFe-alloy with partial substitution of Fe by Ti and Mn. *J. Alloy. Compounds.* **2021**, *874*, 159925. [CrossRef]

60. Kölbig, M.; Bürger, I.; Linder, M. Thermal applications in vehicles using Hydralloy C5 in single and coupled metal hydride systems. *Appl. Energy* **2021**, *287*, 116534. [CrossRef]